

Keck Infrared Observations of Jupiter's Ring System near Earth's 1997 Ring Plane Crossing

Imke de Pater

Astronomy Department, University of California, 601 Campbell Hall, Berkeley, California 94720
E-mail: imke@floris.berkeley.edu

Mark R. Showalter

Center for Radar Astronomy, Stanford University, Stanford, California 94305

Joseph A. Burns and Philip D. Nicholson

Astronomy Department, Cornell University, Ithaca, New York 14853

Michael C. Liu

Astronomy Department, University of California, 601 Campbell Hall, Berkeley, California 94720

Douglas P. Hamilton

Astronomy Department, University of Maryland, College Park, Maryland 20742-2421

and

James R. Graham

Astronomy Department, University of California, 601 Campbell Hall, Berkeley, California 94720

Received April 20, 1998; revised October 1, 1998

We imaged the jovian ring system at a wavelength of $2.27 \mu\text{m}$ with the 10-m W. M. Keck telescope on August 14 and 15, 1997, when the ring plane was almost edge-on (opening angle $\beta = 0.17^\circ$) and near opposition (phase angle $\alpha \approx 1.1^\circ$). The resolution in the images is $0.6'' = 0.025 R_J$. We obtained the first images of the jovian halo and gossamer ring in back-scattered light, and the best ground-based images to date of Jupiter's main ring. The main ring is radially confined between 1.70 and $1.82 R_J$ (where $1 R_J = 71398 \text{ km}$), with a maximum (after inversion) at $1.79 R_J$, in agreement with the Voyager findings. The halo extends inward from the main ring (at $1.71 R_J$) down to $1.40 R_J$, apparently bounded by the locations of Lorentz resonances. Roughly 50% of the halo's intensity originates from a region within $\sim 700 \text{ km}$ from the equatorial plane, although it is visible up to $\sim 10,000 \text{ km}$ above and below the plane. Although the vertical extent agrees with Voyager findings, the halo's intensity relative to that of the main ring in the Keck images is much less than in forward-scattered Voyager images, which we attribute to a predominance of micrometer-sized particles, which scatter visible light preferentially in the forward direction. The gossamer ring is found to have two components, with steep dropoffs in brightness at the orbits of Amalthea and Thebe. The first, Amalthea's gossamer ring, is visible between the main ring's periphery and $\sim 2.55 R_J$;

it is relatively uniform in brightness and has a vertical thickness (FWHM) of $0.06 R_J$, clearly broader than the FWHM of the main ring ($0.045 R_J$) and the image resolution. The other component, Thebe's gossamer ring, is a factor of five fainter than Amalthea's ring and about twice as broad vertically (FWHM $\approx 0.12 R_J$). This ring extends outward to $3.11 R_J$, but additional material is visible, albeit barely, out to $\sim 3.6 R_J$, near the edge of our images. The vertical extent of both the Thebe and Amalthea rings decreases with decreasing distance to the planet. © 1999 Academic Press

Key Words: Jupiter; ring; infrared; dust; dynamics; photometry.

1. INTRODUCTION

Jupiter's ring was first detected, although indirectly, by Pioneer 11, when charged particle detectors experienced sudden drops in the energetic particle fluxes in the region 1.7 – $1.8 R_J$ ($1 R_J = 71,398 \text{ km}$, 1 jovian radius at the 1-bar level; Smoluchowski 1976) (Fillius *et al.* 1975). The first image of the ring, in back-scattered light, was obtained by Voyager 1, which was followed by two dozen Voyager 2 images (Owen *et al.* 1979, Jewitt and Danielson 1981, Burns *et al.* 1984, Showalter

et al. 1985, 1987). The latter spacecraft obtained images both in forward- and back-scattered light. Subsequent to the Voyager detections, several researchers succeeded in obtaining ground-based measurements of the ring, the earliest of which were obtained by Becklin and Wynn-Williams (1979) at near-infrared wavelengths, Smith and Reitsema (1980) at visible wavelengths, and Neugebauer *et al.* (1981) both at $0.889 \mu\text{m}$ and in the infrared between 1.6 and $2.4 \mu\text{m}$. Jewitt *et al.* (1981) published the first groundbased *image* of the main ring ansae at $0.889 \mu\text{m}$, followed in 1991 by near-infrared images of the main ring and associated small satellites Metis and Adrastea by Nicholson and Matthews (1991). Recently, Galileo has imaged the ring in forward-scattered light (Ockert-Bell *et al.* 1999).

In Voyager images the jovian ring was much brighter in forward- than in back-scattered light, suggesting a large population of micrometer-sized and submicrometer-sized dust. The

ring appears to consist of three components (Burns *et al.* 1984, Showalter *et al.* 1985, 1987): a narrow *main ring*, roughly 7000 km wide, with an abrupt outer boundary at $1.81 R_J$, a more gradual inner boundary at $1.72 R_J$, and a normal optical depth $\tau \approx \text{few} \times 10^{-6}$. Interior to the main ring lies the *halo*, which consists of a radially confined torus of faint material, with an inner boundary at $\sim 1.4 R_J$ and $\tau \approx 10^{-6}$. The halo's full vertical thickness was measured to be $\sim 2 \times 10^4 \text{ km}$ (Showalter *et al.* 1985). The third component of the ring system is the extremely tenuous *gossamer ring* ($\tau \sim 10^{-7}$), which extends from just exterior to the main ring outward to at least $\sim 3 R_J$, well beyond Amalthea's orbit.

As indicated by the optical depths given above, the jovian ring system is extremely faint; its precise structure and the nature of the ring particles are thus poorly known. Observations in forward-scattered light are sensitive mainly to micrometer-sized

Jovian ring ($2.268 \mu\text{m}$)

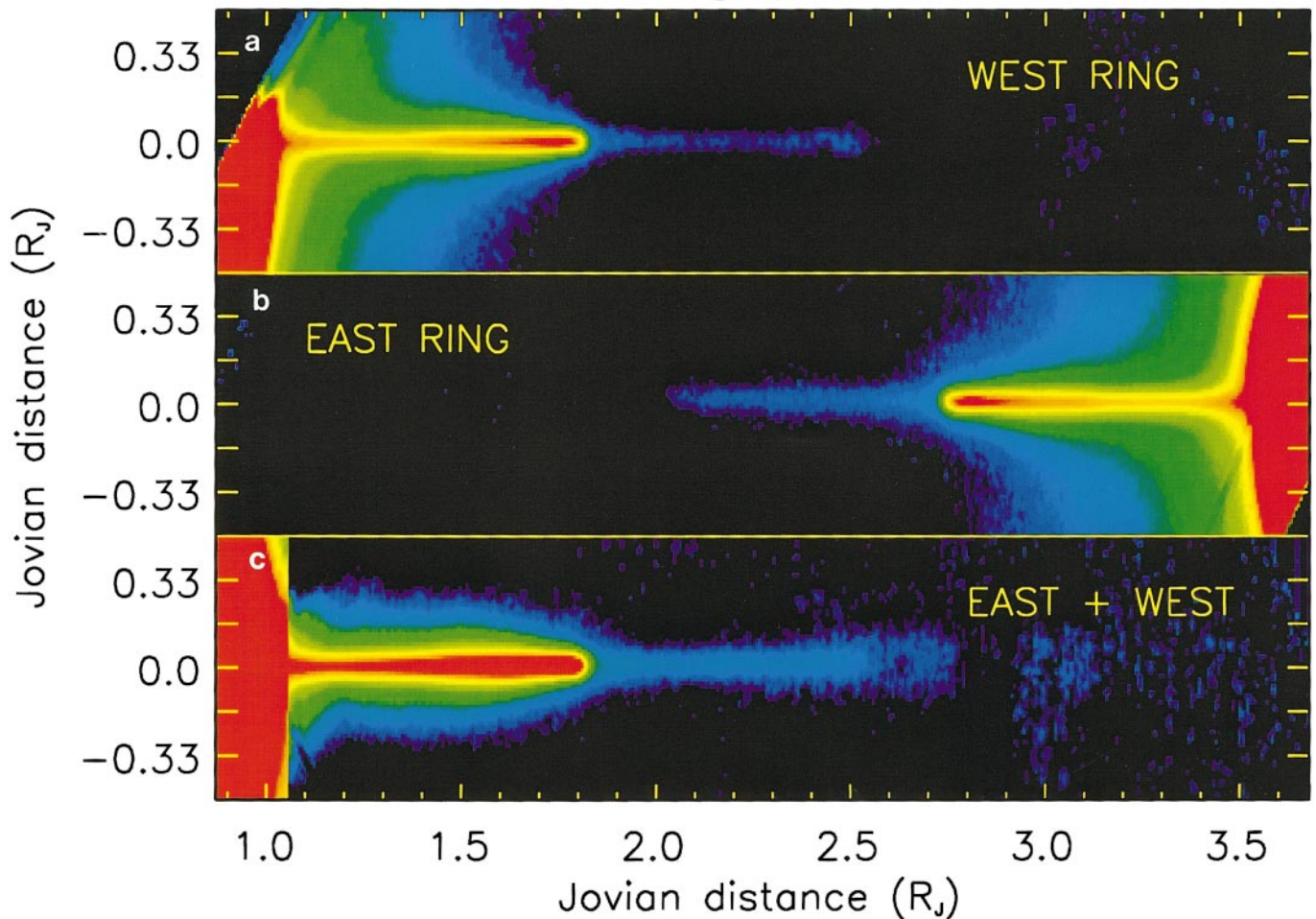


FIG. 1. The jovian ring system as imaged by the W. M. Keck telescope at a wavelength of $2.27 \mu\text{m}$. (a) and (b) show the west and east side of the ring, respectively, while (c) shows the sum of the two rings, after the east ring was “flipped” and the background emission subtracted (see text). The intensity in the latter image is twice that in the individual images to emphasize the gossamer ring.

grains, while measurements in back-scattered light give information on larger-sized grains and macroscopic bodies. “Spectra” of the rings and variations in intensity with phase angle provide clues as to the material composition and the size distribution of the particles, both of which constrain the origin of the rings. Since the lifetimes of micrometer-sized grains are brief (Burns *et al.* 1980, 1984, 1999), the rings must be young and continually replenished with material, although the precise mechanisms of birth and death are disputed.

To improve our understanding of the jovian ring system, we observed the rings during the time that Earth was near the ring plane and near opposition in August 1997. Observations were also made during the actual ring plane crossing in October 1997, but will be described elsewhere. In this geometry, optically thin rings that are confined to the equatorial plane (main ring, gossamer ring) are much brighter than under normal viewing conditions, when the ring opening angle is on the order of $\beta = 3^\circ$. In addition, the edge-on geometry makes it easier to extract the vertical structure of the halo and any north–south asymmetries, if present. In this paper we report our first set of observations, obtained near jovian opposition in August 1997, at a wavelength of $2.27 \mu\text{m}$.

2. OBSERVATIONS

We observed Jupiter’s ring system on UT 1997 August 14 and 15 using the 10-m W. M. Keck telescope¹ on Mauna Kea, Hawaii. The opening angle of the rings was 0.17° on both days, and the planet’s phase angle was 1.07° on August 14 and 1.28° on August 15. At this opening angle, the projected minor axis of the main ring is $\leq 0.3''$. The seeing was $\sim 0.6''$ on both days so the rings are effectively seen edge-on. We used the facility’s near-infrared camera (Matthews and Soifer 1994), which is equipped with a 256×256 pixel Santa Barbara Research Corporation InSb array. The pixel size is $0.151''$, corresponding to 444 km at Jupiter. The observations were carried out with a filter centered at a wavelength $\lambda = 2.268 \mu\text{m}$ ($2.190\text{--}2.345 \mu\text{m}$). Sunlight, usually reflected by Jupiter’s thick cloud layers, is absorbed at this wavelength by methane gas above the main cloud deck, making the planet very dark and greatly reducing scattered light near the rings.

On UT August 14 we observed the west side of Jupiter’s ring, and on August 15 the east side. These days were carefully chosen to avoid interference by reflections from Galilean moons. Observational sequences were designed to take five images of Jupiter’s ring, each shifted in position by a few arcseconds to avoid the superposition of bad pixels. In between two sets of five images, we moved $200\text{--}240''$ north or south to measure the sky. This was also done in sets of five images, each shifted by $10''$ so that stars were deleted when we median-filtered the frames. We

typically integrated for 20 s per exposure, although exposures targeted at the gossamer ring were 60 s long.

We linearized and flat-fielded the data according to standard procedures (Graham *et al.* 1994). The absolute calibration of the images was set by observing the HST IR standard stars SJ9101 and SJ9182, which have K-band ($\lambda = 2.24 \pm 0.23 \mu\text{m}$) magnitudes of 11.223 ± 0.008 and 11.082 ± 0.010 , respectively (Persson *et al.* 1998). The K-band flux density from a zero-magnitude star is 646 Jy ($1 \text{ Jy} = 10^{-26} \text{ W m}^{-2} \text{ Hz}^{-1}$). We measured the extinction coefficient for each night by observing the standards over a range of airmasses. At one airmass, one count/s corresponded to a flux density of $0.161 \mu\text{Jy}$ on August 14, with an extinction coefficient of 0.1 mag/airmass. On August 15 one count/s corresponded to $0.167 \mu\text{Jy}$, with an extinction coefficient of 0.03 mag/airmass. Observations of the stars suggest our calibration uncertainty to be $\leq 3\%$.

To compare our measurements with previous results and physical models, we convert from units of Jy/pixel to the dimensionless ratio I/F . Here I is the reflected intensity, and πF is the incident solar flux density at Jupiter at the wavelength of observation. By this definition, $I/F = 1$ for a perfectly diffusing “Lambert” surface when viewed at normal incidence. We recall that the solar flux density at Jupiter (5.061 AU on these dates), $F = 1.451 \times 10^{-14} \text{ W m}^{-2} \text{ Hz}^{-1} = 1.451 \times 10^{12} \text{ Jy}$ at $\lambda = 2.27 \mu\text{m}$ (Arveson *et al.* 1969). Note that values of I/F are independent of geocentric distance and can be readily compared with those at other wavelengths because the solar spectrum has been removed.

3. RESULTS

3.1. Images

All frames were rotated during the processing so that Jupiter’s north pole was up, and the rings horizontal in the images. We carefully aligned all images using the predicted positions (offsets from Jupiter) of the moons Amalthea, Thebe, Metis, or Adrastea (JPL, Horizons ref. orbit JUP059). Positional tests with pairs of moons showed that the ephemerides of all moons (including Adrastea) are remarkably good. In moonless frames we employed the half-power point of the outer edge of the main ring to align the images in the east–west direction. We used a simple Gaussian fit to the main ring to adjust the vertical alignment of all images. After aligning all images, the moons, stars, and any remaining bad pixels were removed from the images, prior to coadding the data. Our final image size was 500×400 pixels.

The averaged images from August 14 and August 15 are shown in Figs. 1a and 1b, respectively. The main ring (red) and halo (yellow–green–blue) are clearly visible on the images, as well as the gossamer ring (blue–violet) between 1.8 and $2.5 R_J$. No asymmetries are noted between the east and west ansae, nor in the north–south direction. To improve the signal-to-noise (S/N), we therefore ‘flipped’ the east ansa from east to west, and averaged the east and west sides together. The extent of the halo was determined from vertical scans through this combined

¹ The W. M. Keck telescope is jointly owned and operated by the University of California and the California Institute of Technology.

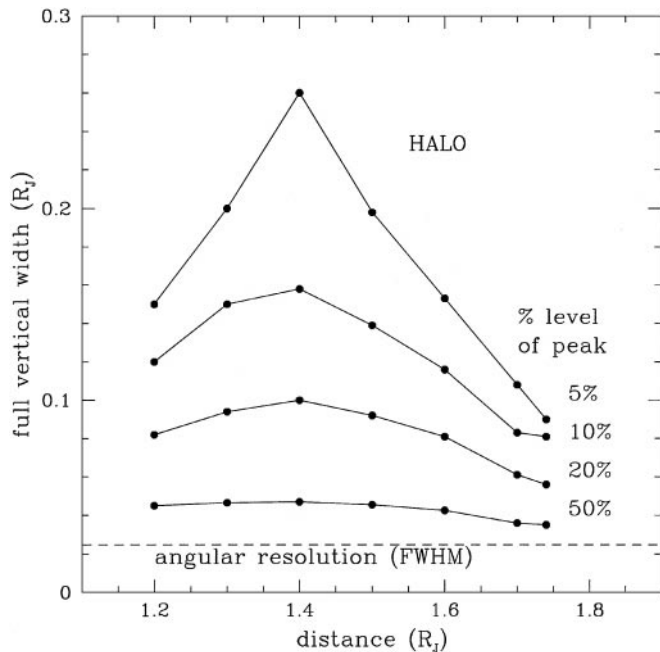


FIG. 2. The full extent of the main ring and halo (from the combined image, Fig. 1c, before the background was subtracted) at 5, 10, 20, and 50% of the peak intensity along a vertical scan that crosses the equatorial plane at the radial distance is indicated. For each scan, the background was determined and subtracted. For comparison, we indicate the angular resolution or seeing (FWHM) by a dashed line.

image, where for each scan an average background level was estimated from the values at large distances ($\geq 0.4 R_J$) north and south of the ring. This background level was subtracted for each scan individually. The result is shown in Fig. 2. The full extent of the halo is $\sim 16,000$ km ($\approx 0.22 R_J$) at the 5% level of the peak intensity, which is compatible to the value measured by Voyager in forward-scattered light (Burns *et al.* 1984, Showalter *et al.* 1987).

As shown in Figs. 1a and 1b, scattered light from the planet dominates the emissions close to Jupiter, and also affects the rings at larger distances. Since Jupiter is characterized by zonal bands, with a very strong, ~ 0.35 – $0.4 R_J$ wide, band centered near the equator at this wavelength, it is important to determine a “background” radial profile from scans parallel and as close as possible to the rings. We constructed such a profile from five rows just north and south of the halo (25 – 29 pixels = 0.155 – $0.180 R_J$ from the mid-plane), to represent the background as accurately as possible, but such that we do not overlap with the halo (Fig. 2). We constructed a “background image” from this profile by setting each row in a 500×400 pixel image equal to the radial background profile. This background image was subtracted from the averaged “observed” image, the result of which is shown in Fig. 1c. This figure clearly shows the main ring, halo, and gossamer ring, without the confusion of Jupiter’s scattered light. We used this image in the analysis described below.

3.2. Edge-on Profiles

Figure 3 displays edge-on radial profiles extracted from the ring image displayed in Fig. 1c. To enhance the S/N , we Hanning-smoothed² all radial profiles shown (i.e., in Figs. 3a, 3b, and 6a, 6b). The lower solid curve in Fig. 3a shows a profile integrated over the inner five rows centered on the ring plane, i.e., over $0.75''$ ($=0.03 R_J$). This profile thus represents the edge-on radial profile of the main ring. The upper solid curve is integrated over $5.9''$ ($=0.24 R_J$), and thus represents a profile of the vertically integrated halo plus main ring. The dashed line is the $0.75''$ strip after the peak intensity at $1.73 R_J$ is scaled to the $1.73 R_J$ intensity in the $5.9''$ strip.

We note that the intensity in both strips drops dramatically going outward between 1.73 and $1.81 R_J$, and in the $0.75''$ strip, it decreases more gradually toward smaller jovian radii. This suggests, in agreement with Voyager data, that the main ring is confined to a narrow range of radii. However, since we view the ring nearly edge-on, the peak brightness in these profiles is displaced inward from the brightness maximum measured by Voyager ($1.79 R_J$; Burns *et al.* 1984, Showalter *et al.* 1987). The $5.9''$ strip looks very different than the $0.75''$ strip inward from the ring ansa and suggests that, in projection, the halo extends inward from $1.68 R_J$. Assuming that the peak intensity at $1.73 R_J$ is due only to the main ring, the difference between the $5.9''$ and scaled $0.75''$ strips suggests that at least 30% of the vertically integrated intensity at $1.4 < r < 1.68 R_J$ can be attributed to the halo. We say at least 30% since the halo emission from near the ring plane has been counted as main-ring emission in this approach, as has the (minor) contribution of the gossamer ring. The abrupt change in slope at $1.4 R_J$ in both profiles suggests this is the inner boundary of the halo. We superposed the locations of the moons Metis and Adrastea, as well as the locations of the Lorentz 2:1 and 3:2 resonances on the figure. These will be discussed in more detail in Section 4.

Figure 3b shows edge-on profiles across the region of the gossamer ring. The solid line shows an average over $0.75''$ ($=0.03 R_J$), centered narrowly about the equator, while the dashed line shows an average over $3.17''$ ($=0.13 R_J$). Note that the intensities of the two scans are practically equal beyond $2.55 R_J$, while the broader scan is at about half the intensity level of the narrower scan at $r < 2.5 R_J$. Both profiles show abrupt decreases in intensity in the vicinity of $2.55 R_J$, the orbit of the moon Amalthea. Beyond $3.11 R_J$, near Thebe’s orbit, the average intensity drops again, a feature which may be more obvious in Fig. 4b (discussed below). In this figure a vertical scan is shown through the ring, averaged between 2.65 and $3.11 R_J$ (solid line), and 3.15 and $3.60 R_J$ (dashed line). This figure, the edge-on profile in Fig. 3b, and the image in Fig. 1c, show that the ring is still “visible” at $r > 3.11 R_J$, albeit barely above the

² Hanning smoothing is usually used in spectral line observations and consists of applying a running 3-pixel boxcar average across the scan, where the 3 pixels are weighted as 0.5, 1, and 0.5.

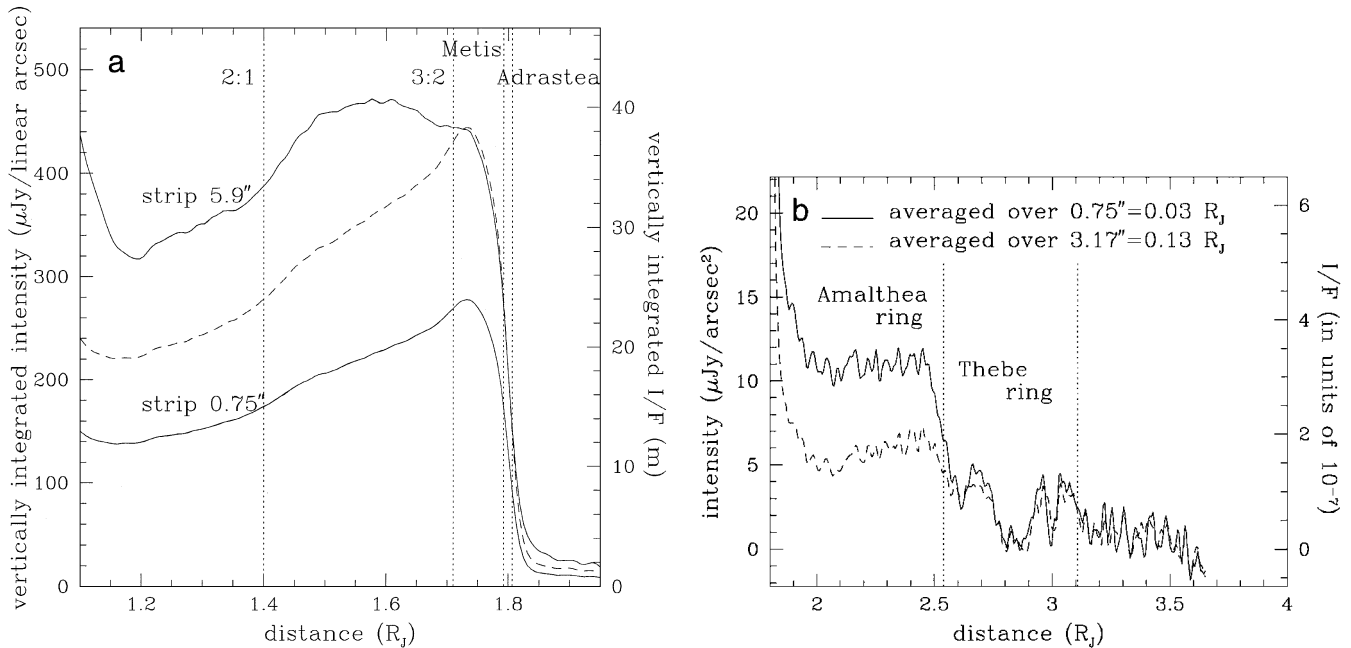


FIG. 3. (a) Edge-on radial scans along the ring plane, integrated vertically over $0.75'' = 0.03 R_J$ (5 rows, lower solid line) and $5.9'' = 0.24 R_J$ (39 rows, upper solid line). The dashed line is the $0.75''$ strip scaled in intensity to that of the $5.9''$ strip at $1.73 R_J$. The orbits of the moons Metis and Adrastea, as well as the locations of the 2:1 and 3:2 Lorentz resonances, are indicated. (b) Edge-on radial profile along the gossamer rings, averaged vertically over $0.75'' = 0.03 R_J$ (5 rows, solid line) and $3.17'' = 0.13 R_J$ (21 rows, dashed line). The locations of the orbits of Amalthea and Thebe are indicated.

background. To correspond with the Galileo terminology (Ockert-Bell *et al.* 1999), we will call the part of the gossamer ring inward of Amalthea’s orbit the “Amalthea ring” ($\approx 2.55 R_J$), and that inward of Thebe’s orbit ($\approx 3.11 R_J$) the “Thebe ring.” The Thebe ring alone is visible between 2.55 and $3.11 R_J$, whereas both rings are superposed in our data at $r < 2.55 R_J$; however, because the Thebe ring is much fainter, the intensity at 1.8 – $2.55 R_J$ is dominated by the Amalthea ring. Similarly, inside of $1.8 R_J$ the gossamer rings are overshadowed by the main ring.

One may note in Figs. 1c and 3b that there are several dips in intensity (in contrast to the abrupt drops at 2.55 and $3.1 R_J$) between 2.6 and $3.1 R_J$. In addition, the S/N is lower at these larger distances, because fewer frames were centered here. The satellite Thebe had to be removed from several of the images in the region 2.6 – $3.1 R_J$, and we suspect that this may have influenced the resulting intensity profile. Because a dip in the edge-on profile of an optically thin ring is physically implausible, and because we suspect that the removal of Thebe influenced the profile, we ignore these dips in the gossamer ring.

Figure 4 shows vertical scans through the gossamer ring at various radial positions. The solid and dashed lines in Fig. 4a are scans through the Amalthea ring, averaged over 15 pixels or $0.1 R_J$ (solid line is centered at $2.44 R_J$, dashed line is centered at $2.05 R_J$), and the dotted line is a scan through the Thebe ring (averaged between 2.65 and $3.11 R_J$). An enlarged view of the Thebe ring is shown in Fig. 4b (solid line), where the dashed line shows a vertical scan outside of Thebe’s ring, averaged over

3.15 – $3.60 R_J$. Similar profiles, although of poorer S/N , are obtained when averaging over 10–25 pixels at different positions between 3.15 and $3.60 R_J$, which suggests that material is present out to at least $3.60 R_J$. The FWHM of the Amalthea ring is about half that of the Thebe ring, a feature which can also be seen in the difference between the solid and dashed curves in Fig. 3b. Note that the total thickness of the Thebe ring in Fig. 4a is similar to that of the outer Amalthea ring at intensities $S < 2 \mu\text{Jy}/\text{arcsec}^2$; that is to say, the shoulders seen in the Amalthea scan are due to background Thebe material. We further note that the Amalthea ring gets narrower moving inward from Amalthea’s orbit, and so is the total width, i.e., that part of the scan which is due to the Thebe ring. The latter feature is best seen from Fig. 1c, where the faint Thebe ring is clearly wedge-shaped, being broadest at $2.7 R_J$ (and presumably even broader at $3 R_J$), narrowing linearly moving inward to $\sim 2 R_J$, where the main ring starts to overwhelm the profile.

3.3. Ring Inversions

3.3.1. Inverted image. Since the rings are optically thin and edge-on, we can, by assuming the spatial distribution of the rings to be cylindrically symmetric, invert the image in Fig. 1c by using an “onion-peel” deconvolution method (Showalter *et al.* 1987). We assume that each row in the image represents an edge-on radial profile of the rings. Starting from the outer edge in each row, the intensity of the outermost zone is determined and then subtracted from the radial profile in that row, before

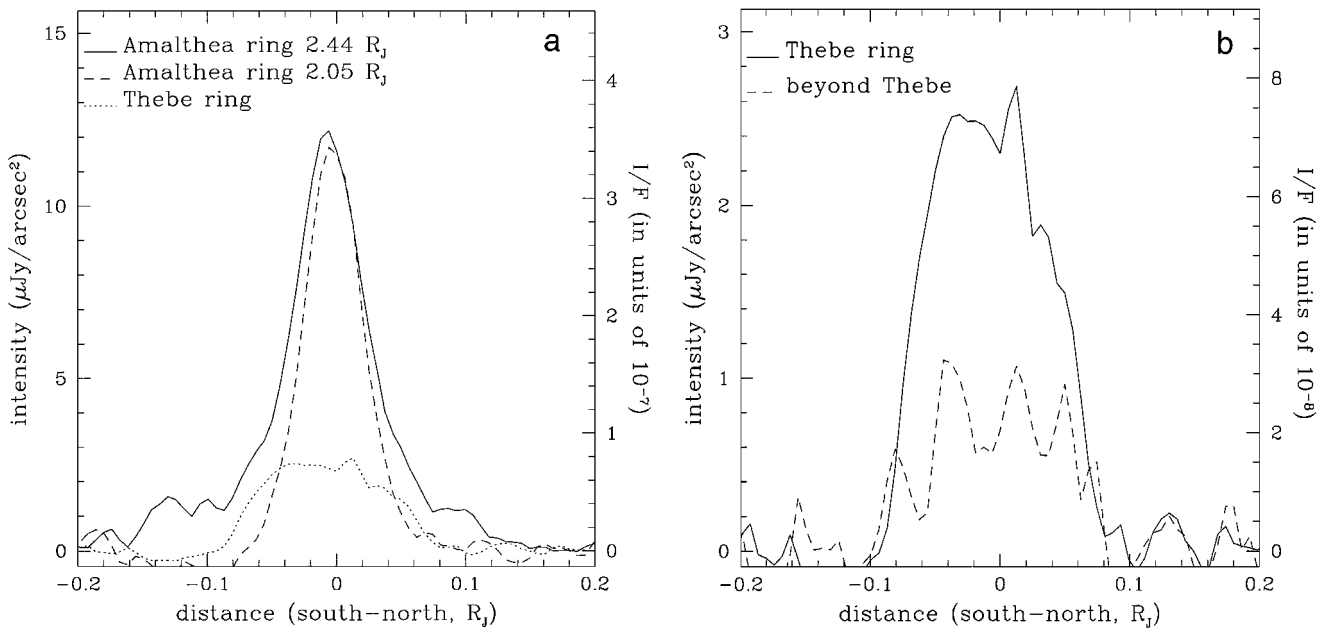


FIG. 4. (a) Vertical scans through the gossamer ring: two scans through the Amalthea ring are shown, each integrated over 15 columns ($2.27''$). The solid line is centered at $2.44 R_J$, the dashed line at $2.05 R_J$. The dotted line is a scan averaged over the entire Thebe ring, between 2.6 and $3.11 R_J$. (b) The solid line shows a vertical scan through the Thebe ring, equal to the dotted line in (a); the dashed line is a scan through the ring beyond Thebe, averaged over 3.15 – $3.60 R_J$.

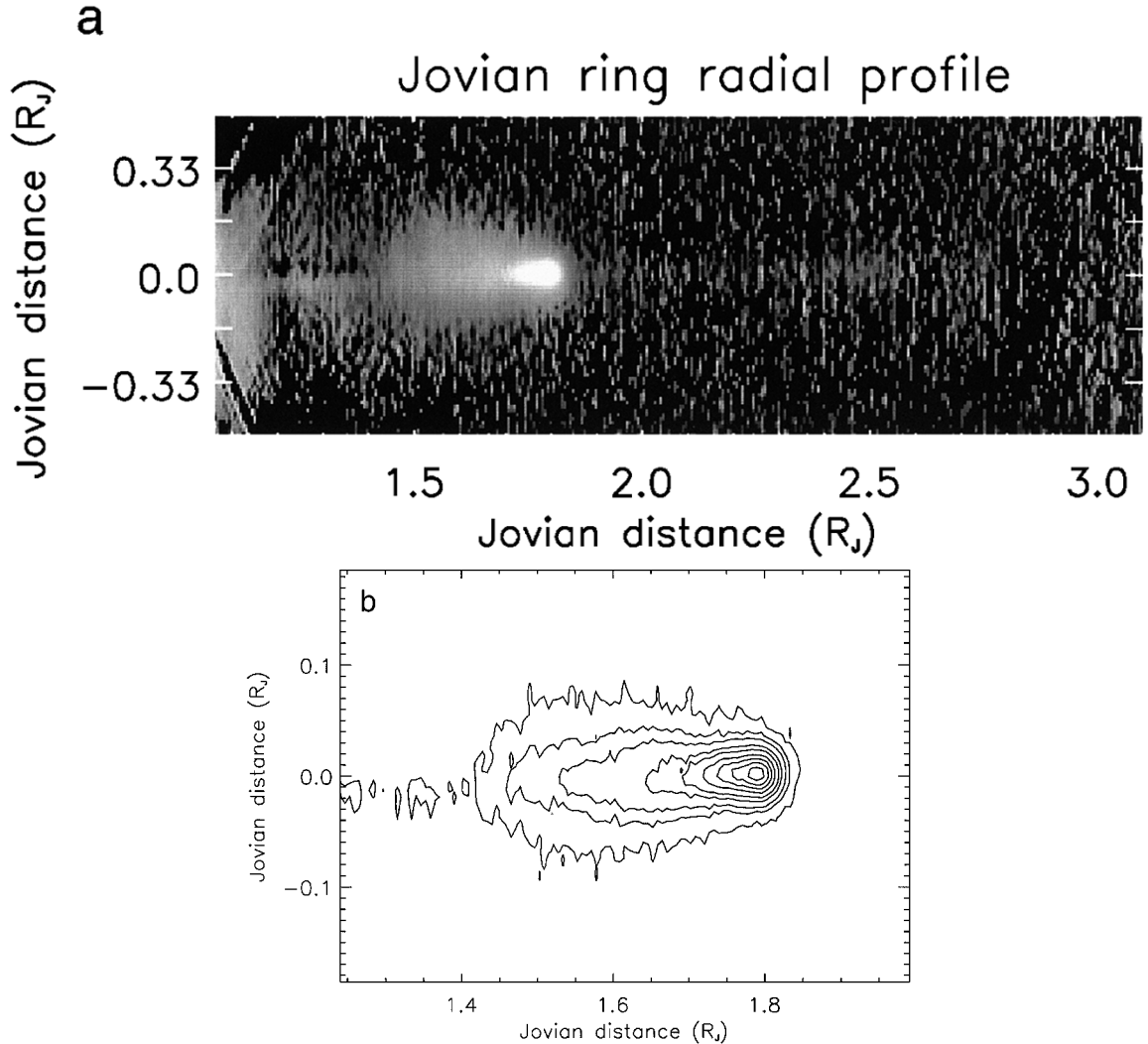


FIG. 5. (a) Image of Jupiter's ring system after applying the inversion technique described in the text. This image thus provides a radial cross-section of the ring, without the effects due to line-of-sight integration. (b) A contour map of the main ring and halo, where the levels are $0.07, 0.16, 0.26, 0.46, 0.65, 0.98, 1.3, 1.6,$ and $1.95 \times 10^{-10} I/F$ per km; the maximum in the images is $2.18 \times 10^{-10} I/F$ per km.

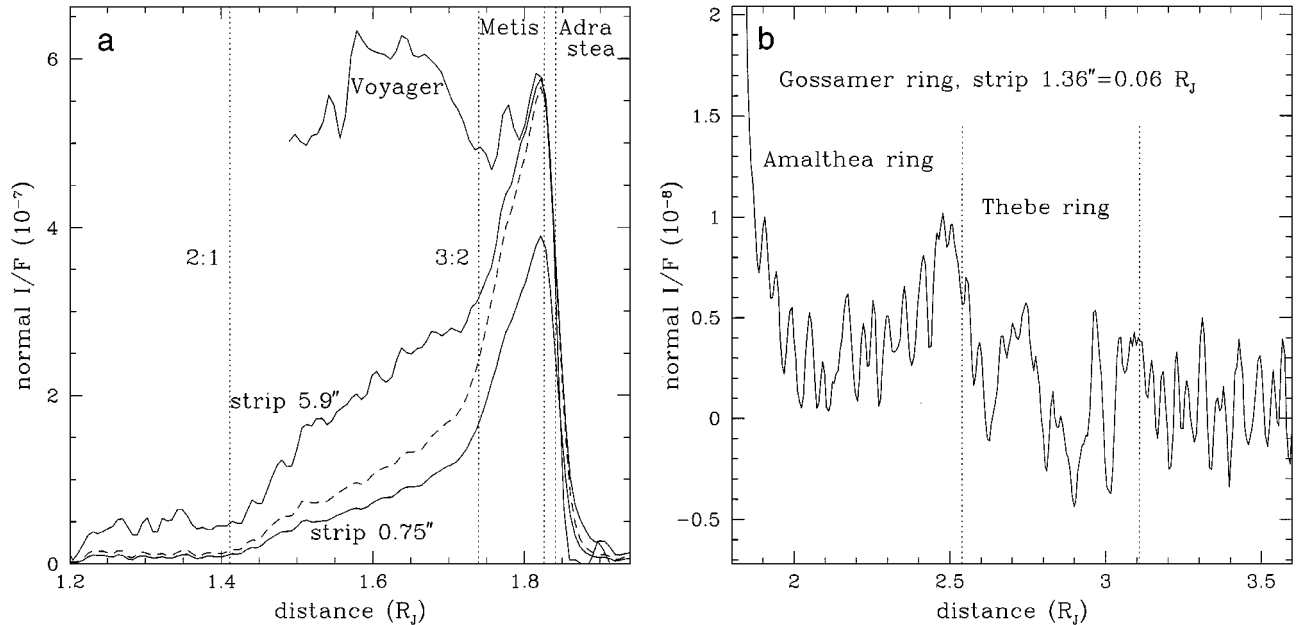


FIG. 6. Radial profiles along the ring plane, through the inverted image displayed in Fig. 5a. (a) Radial scans through the main ring and halo, integrated vertically over $0.75'' = 0.03 R_J$ (5 rows, lower solid line) and $5.9'' = 0.24 R_J$ (39 rows, middle solid line). The dashed line is the $0.75''$ strip scaled in intensity to that of the $5.9''$ strip at $1.79 R_J$. The upper solid line is the Voyager profile, scaled also to the intensity of the $5.9''$ strip at $1.79 R_J$. The orbits of the moons Metis and Adra stea, as well as the locations of the 2:1 and 3:2 Lorenz resonances, are indicated. (b) Radial profile through the gossamer ring, integrated vertically over $1.36'' = 0.06 R_J$ (9 rows). This profile was binned (every two points were combined) and Hanning smoothed to increase the S/N . The locations of the orbits of Amalthea and Thebe are indicated.

the next inner zone is defined, etc. This method thus works on a pixel-by-pixel basis. Because it is akin to differentiation, it can only be applied successfully because of the very high signal-to-noise ratio in the original image (Fig. 1c). The resulting inverted image is shown in Fig. 5a. This image thus represents the true radial distribution of the rings, where all line-of-sight effects have been removed. The very bright main ring is surrounded by the much fainter halo. The halo becomes wider or thicker inward of $1.71 R_J$ (see also the contour map in Fig. 5b). The halo extends inward to $\sim 1.4 R_J$. Inside of $1.4 R_J$ there is a slight artifact, visible as negative intensities just above the ring plane, and positive intensities just below. This is probably caused by imperfect cancellation of the main ring's bright pixels during the inversion process. Extending outward from the edge of the main ring one can see, although barely, the Amalthea ring. This ring is clearly brightest near its outer edge at $2.5 R_J$. Unfortunately, the Thebe ring is too faint to appear in this representation.

3.3.2. Radial profiles. In analogy to Fig. 3, Fig. 6 shows radial profiles through the inverted image in Fig. 5a. Again, in Fig. 6a we show profiles integrated vertically over $0.75'' (=0.03 R_J)$ (lower solid line) and $5.9'' (=0.24 R_J)$ (middle solid line), where the dashed line is the $0.75''$ strip scaled to the peak intensity of the $5.9''$ strip. A check on the consistency of the inversion procedure is provided by the observation that at the innermost radii the intensity in both Keck profiles returns to near-zero, in particular for the narrow strip, where the S/N for

each row in the original image (Fig. 1c) was high. The main ring is clearly visible as a narrow band between 1.70 and $1.82 R_J$, peaking at $1.79 R_J$, near or just interior to the orbit of Metis ($1.7922 R_J$). A change in slope or flattening in the profile is visible between 1.74 and $1.77 R_J$. The $0.75''$ strip, which represents primarily the main ring, shows a gradual inward decline in intensity from about 30% of the peak intensity at $\sim 1.70 R_J$ to essentially zero at $1.40 R_J$. The $5.9''$ strip, which represents the main ring plus the halo, shows an intensity at $1.70 R_J$ of roughly $\sim 50\%$ of the peak intensity, but also drops to near zero at $1.40 R_J$. The difference between the two profiles represents light from the vertically extended halo, away from the equatorial plane; thus we conclude that the halo's inner boundary is at $1.40 R_J$, and that the halo extends outward to $1.71 R_J$, brightening all the way. Roughly half of the halo brightness originates from within ~ 1000 km of the equatorial plane ($0.75''$ strip between 1.4 and $1.70 R_J$), while the halo extends out to $\sim 10,000$ km from the equatorial plane (Fig. 2).

Because the original image can be calibrated in units of I/F and because the geometry is well known, it is possible to calibrate the profiles shown in Fig. 6. The vertical axis is in units of "normal I/F ," equivalent to the I/F that would be observed looking directly down through the ring plane, but at the given phase angle of 1.1° . In the main ring, the peak normal I/F is $4-6 \times 10^{-7}$ (depending on the width of the strip). This compares very favorably to the value of 4×10^{-7} measured at $2.2 \mu\text{m}$ and $\alpha = 2.2^\circ$, after correction to normal viewing, by Nicholson

and Matthews (1991). The value is substantially larger than the main ring's intensity at visual wavelengths, where normal $I/F = 1.5 \times 10^{-7}$ (Showalter *et al.* 1987). This confirms the red color inferred by Showalter *et al.* from the Voyager images, and extended to the near-IR by Neugebauer *et al.* (1981) and Nicholson and Matthews (1991).

The upper solid line in Fig. 6a is the vertically integrated radial profile as measured by Voyager (frame 20693.02; Showalter *et al.* 1987). We scaled this profile to the $5.9''$ strip Keck intensity at $1.79 R_J$. All profiles show a sharp drop in intensity just beyond the orbit of Metis. Inside of $1.79 R_J$, where the Keck profiles showed a change in slope or flattening in intensity at 1.74 – $1.77 R_J$, the Voyager profile exhibits an enhancement in intensity. The Voyager profile further displays a pronounced increase in intensity inward of $1.71 R_J$, which can be attributed to the halo. The inner edge of the halo, however, was not well defined. Since the Keck profiles were taken in back-scattered light (at phase angle $\alpha \approx 1.1^\circ$), and the Voyager profile in forward-scattered light ($\alpha = 174^\circ$), we attribute the difference between the halo profiles to the fact that different groups of particles are highlighted at these very different phase angles. Because the halo is so bright in forward-scattered light, the particles in the halo are thought to be (sub)micrometer-sized material (Showalter *et al.* 1987). In a future paper we will use all this information, augmented by the Galileo data and Keck measurements at different phase and ring inclination angles, to constrain particle properties in terms of size distribution and composition.

A radial scan through the gossamer rings is shown in Fig. 6b. This scan is integrated over the full thickness at half power (FWHP = $1.36'' = 0.06 R_J$) to maximize the S/N . The intensity of the Amalthea ring increases steadily from $\sim 2 \times 10^{-9}$ at $2 R_J$ up to $\sim 10^{-8}$ at $2.5 R_J$; beyond $2.5 R_J$ the intensity drops to near-zero. The ring's peak normal I/F is approximately 1×10^{-8} , ~ 60 times fainter than the main ring. This is rather similar to the ratio found from Voyager data. The Thebe ring is too faint for the inversion process to work.

3.4. Moons

We searched for hidden moonlets in the rings by subtracting our overall ring images (Figs. 1a and 1b) from the individual frames (roughly 100 frames for each ansa). As expected, the known moons Amalthea, Thebe, Metis, and Adrastea were clearly visible, but no smaller moonlets were found. The measured flux densities and corresponding K magnitudes for Thebe, Metis, and Adrastea (Amalthea was partially saturated in the frames) are summarized in Table I. The mean reflectance (I/F) of each satellite at $\lambda = 2.27 \mu\text{m}$ is also given here, calculated using the average radii derived from Galileo images (Thomas *et al.* 1998). Comparison with the Galileo (GLL) visible albedos (I/F_{vis} in the table, from Thomas *et al.* 1998) shows that all three moons are quite red in color, especially Metis and Adrastea. Thebe's albedo at $2.2 \mu\text{m}$ is very similar to that of Amalthea ($p_K = 0.09$, Neugebauer *et al.* 1981). The color of Jupiter's ring is close to that of the two small satellites.

TABLE I
Satellite Photometry

Satellite	F_V (mJy)	K mag. ^a	R (km)	I/F_{vis}	I/F^a
Thebe	3.18 ± 0.1	13.27 ± 0.03	49.3	0.049 ± 0.005	0.105 ± 0.003
Metis	1.24 ± 0.08	14.3 ± 0.1	21.5	0.063 ± 0.006	0.21 ± 0.02
Adrastea	0.18 ± 0.03	16.4 ± 0.2	8.2	0.10 ± 0.05	0.22 ± 0.04

^a Measured with a 2.19 – $2.35 \mu\text{m}$ filter, rather than a standard 2.0 – $2.4 \mu\text{m}$ K filter.

We estimate an upper limit of 0.05 mJy on hitherto unseen moonlets within the main ring, and ~ 0.02 mJy in the gossamer ring. This suggests that there are no moons in Jupiter's main ring, other than Metis and Adrastea, larger than ~ 4.5 km in radius, and none larger than 3 km in the gossamer ring (assuming an albedo equal to that of Adrastea). A typical rms noise level in the separate images is on the order of 3 – $4 \mu\text{Jy}$.

4. DISCUSSION

4.1. Main Ring and Halo

Since first noticed, the vertical extent of the halo has been used to argue that the dynamics of the grains are heavily influenced by electromagnetic forces, implying that the halo consists only of small particles. This, of course, agrees with the interpretation of the halo's photometry. It is also consistent with results from the main ring's photometry, which indicates that the size distribution of these particles follows a power-law distribution ranging from submicrometer to particles that are tens of micrometers across (Showalter *et al.* 1987). The original belief (Consolmagno 1980, Jewitt and Danielson 1981) was simply that ring particles got pushed around by electromagnetic forces, which required large charge-to-mass ratios to produce significant amplitudes; Burns *et al.* (1985) modified this to incorporate resonant forcing at specific locations where grains would undergo unusually large amplitude motions. Regardless of the precise mechanism, typical charges required submicrometer grains in the halo. Based upon these theories, the halo must consist only of submicrometer-sized dust, and thus these particles, collectively, must produce the back-scattered halo light as observed with the Keck telescope. The "halo" particles in the equatorial plane, however, may consist of a particle size distribution including larger-sized material, just like in the main ring. Because of the low signal-to-noise of most halo data, due to the obscuring main ring, accurate photometric models have not yet been constructed, particularly of any equatorial component.

The strongest vertical Lorentz resonances, the locations where charged dust will experience resonant forces, are found at $1.71 R_J$ (the $3:2$ resonance at $122,150$ km) and $1.40 R_J$ (the $2:1$ resonance at $100,450$ km), positions near where we find the halo's outer and inner boundaries, respectively. Numerical simulations (Schaffer and Burns 1992, Hamilton 1994, Burns *et al.* 1996, Horanyi and Cravens 1996) of charged grains that evolve inward

(perhaps due to Poynting–Robertson drag) through these resonances find that large-amplitude inclinations are induced at these points. It appears that grains that originate in the main ring and evolve inward will be scattered vertically within a region surrounding the 3 : 2 resonance, whose width is a result of the eccentricity jumps at the horizontal cousin of this resonance and due to different charge-to-mass ratios. While the particles continue to evolve, two effects lead to a loss of halo material around $1.4 R_J$. Most importantly, material is affected by the powerful 2 : 1 vertical Lorentz resonance which is significantly stronger than the 3 : 2 resonance responsible for the formation of the jovian halo. The resonance spreads ring material into a much broader halo with lower surface brightness which is difficult to see against Jupiter’s scattered light (see Fig. 6a). In addition, material may also be affected by the 2 : 1 horizontal resonance which causes a sharp increase in orbital eccentricities, thereby causing a direct loss of ring particles to the atmosphere. The observations reported here and by the Galileo team (Ockert-Bell *et al.* 1999) show that the inner and outer boundaries of the halo do coincide with these resonance locations. Despite the apparent absence of material close to the planet in the Keck and Galileo images, the simulations see some material in this region. The fate of larger grains goes unanswered.

4.2. Gossamer Ring

Analyzing the only Voyager image in which the gossamer ring was found, Showalter *et al.* (1985) inferred that the ring’s brightness decayed linearly from the outer periphery of Jupiter’s main ring until it faded into the background, somewhere near or beyond Thebe’s orbit; a 20% enhancement seemed to be present at synchronous orbit. The several Galileo images (Ockert-Bell *et al.* 1999) containing the gossamer ring present quite a different view, probably because of their different viewing geometry. Although all Voyager and Galileo images of the gossamer ring were taken from Jupiter’s shadow, the viewing angles of the two spacecraft were different: the Galileo spacecraft was only 0.15° out of the ring plane, very similar to the Keck viewing angle (0.17°), whereas Voyager was at 2° . We further note that Showalter *et al.* (1985)’s analysis was based on the assumption that the gossamer ring was thin, i.e., confined to the ring-plane like the main ring. In contrast, both the Keck and Galileo data (Ockert-Bell *et al.* 1999) show that the gossamer ring is quite thick, sufficiently so to have significantly altered Showalter *et al.*’s radial profiles.

In the forward-scattered Galileo images, the gossamer ring is seen to have several components, which are quite similar to those present in the Keck images: One band, the Amalthea ring, extends inward from Amalthea and has a nearly uniform intensity and thickness with radius. Another band, the Thebe ring, is of the same character but fainter and thicker and extends inward from Thebe’s orbit. As in the Keck data, there is also a hint of material at greater distances, beyond Thebe. Since the thickness of this material is similar to that of the Thebe ring, the material may be derived from Thebe.

The form of the gossamer ring(s) visible in the forward-scattered Galileo images allows ready interpretation of our (edge-on) profiles seen in back-scattered light (Fig. 3b). The abrupt changes in ring brightness seen at 2.55 and $3.11 R_J$ in Fig. 3b are due to the radially confined rings that are located interior to the orbits of Amalthea ($2.55 R_J$) and Thebe ($3.11 R_J$). The radial profile of the Amalthea ring (Fig. 6b) shows a clear maximum in intensity just inside this moon’s orbit, reminiscent of the bright main ring segment just inside the orbits of Metis and Adrastea.

The vertical extent of the rings, shown in Figs. 1c and 4, reflects the true thickness of the two gossamer rings. Presumably each of the two gossamer rings is composed of material that orbitally evolved inward after leaving the bounding satellite. The difference in thickness is then caused by the difference in inclination angles of the two satellite orbits: 0.4° for Amalthea results in a ring with a thickness of 2320 ± 300 km ($\approx 0.033 R_J$), and 1.1° for Thebe would give a ring of thickness 8620 ± 300 km ($\approx 0.12 R_J$; R. A. Jacobson, personal communication, 1997). Taking our image resolution of $\sim 0.06 R_J$ into account, these numbers agree well with our measured values (Fig. 4) of $\sim 0.11 R_J$ for the Amalthea ring and $\sim 0.17 R_J$ for the Thebe ring (note that this number is representative for the average between 2.65 and $3.15 R_J$, and that the ring will be slightly broader at $3.11 R_J$, due to the wedge-shaped form of the ring). Inside the orbit of Amalthea we thus have both the Amalthea and Thebe rings; both rings are also present inside $1.8 R_J$, but overshadowed by Jupiter’s main ring. The main ring probably formed from material evolving off Metis and Adrastea, an hypothesis reinforced by the similar colors found for Jupiter’s ring, Metis, and possibly Adrastea.

When uncharged particles evolve inward, after coming off the satellite, their orbital inclination angles are preserved; so when evolving inward, the vertical extent of the ring should decrease. Effects like this have been nicely shown in simulations of the orbital evolution of asteroidal dust after the break-up of an asteroid family (Dermott *et al.* 1994). As mentioned in Section 3.2, our data do show that the FWHM of the Amalthea ring is somewhat larger near this moon’s orbit ($2.55 R_J$) than closer in. In addition, in Fig. 1c one can clearly see a wedge-shaped profile for the Thebe ring, being broadest at the largest distances. These effects are compatible with those expected from orbital evolution of dust particles from Amalthea and Thebe. The effect is relatively small, since we look through the edge-on ring, and hence the outer parts of the ring are always superposed on the inner parts.

As mentioned by Burns *et al.* (1984), small satellites may supply more ring material than large satellites, since, even though the surface area increases with radius R^2 , the escape velocity also depends on R , so that a smaller fraction of impact ejecta can escape the larger satellites. Although the Amalthea ring is much brighter than the Thebe ring, the volume of the Thebe ring is $\sim 4\times$ that of the Amalthea ring. The total amount of Thebe ejecta may therefore be comparable to that which has come off Amalthea. A more complete development of a dynamical model

of material evolving off Amalthea and Thebe, as well as a comparison of the Galileo and Keck images, is given by Burns *et al.* (1999).

5. CONCLUSIONS

We have shown data on the jovian ring system in back-scattered light, obtained with the 10-m W. M. Keck telescope in mid-August 1997 when the ring plane was nearly edge-on and the planet was near opposition. The data presented here show, for the first time, the halo and gossamer ring in back-scattered light. These data complement the Galileo data, taken in forward-scattered light (Ockert-Bell *et al.* 1999), and form a crucial piece in understanding the origin and nature of the jovian ring system. Burns *et al.* (1999) describe the dynamics of the gossamer ring particles and how these may evolve off Amalthea and Thebe, based upon a comparison of the Keck and Galileo data. A future paper will present additional Keck data sets, which were taken during ring plane crossing (Oct. 1997) and during times when the rings were completely open (May and July, 1994; August 1998), all at different phase angles. These data can be used with the Galileo data to derive size distributions for the particles in the various ring components. In addition to 2.27- μm observations, the Keck observations contain some spectral measurements, which can be used to extract information on particle composition. Our ultimate goal is to use these measurements to develop a model of the jovian ring system which explains all ground-based and spacecraft data, including the Pioneer 11 observations regarding charged particle absorptions and ground-based radio data on Jupiter's synchrotron radiation, which show the effects of absorption and pitch-angle scattering of high-energy electrons.

ACKNOWLEDGMENTS

We are grateful to the staff of the Keck Observatory and its director, F. Chaffee, for their help in scheduling these observations and their enthusiastic support during the actual observing. This research was supported by NASA's Planetary Astronomy, Geology and Geophysics programs, through Grants NAG 5-4202 to the University of California, Berkeley, and NAGW-544 and NAGW-310 to Cornell University.

REFERENCES

- Arveson, J. C., R. N. Griffith, and B. D. Pearson 1969. Determination of ex-traterrestrial solar spectral irradiance from a research aircraft. *Appl. Opt.* **8**, 2215–2230.
- Becklin, E. E., and C. G. Wynn-Williams 1979. Detection of Jupiter's ring at 2.2 μm . *Nature* **279**, 400–401.
- Burns, J. A., D. P. Hamilton, M. R. Showalter, P. D. Nicholson, I. de Pater, and P. C. Thomas 1999. The formation of Jupiter's faint rings. *Science*, submitted.
- Burns, J. A., L. E. Schaffer, R. J. Greenberg, and M. R. Showalter 1985. Lorentz resonances and the structure of the jovian ring. *Nature* **316**, 115–119.
- Burns, J. A., L. Schaffer, D. P. Hamilton, and M. R. Showalter 1996. The vertical structure of the jovian ring. *Bull. Am. Astron. Soc.* **28**, 1123–1124.
- Burns, J. A., M. R. Showalter, J. N. Cuzzi, and J. B. Pollack 1980. Physical processes in Jupiter's ring: Clues to its origin by Jove! *Icarus* **44**, 339–360.
- Burns, J. A., M. R. Showalter, and G. E. Morfill 1984. The ethereal rings of Jupiter and Saturn. In *Planetary Rings* (R. Greenberg and A. Brahic, Eds.), pp. 200–272. Univ. of Arizona Press, Tucson.
- Consolmagno, G. J. 1980. Electromagnetic scattering lifetimes for dust in Jupiter's ring. *Nature* **285**, 557–558.
- Dermott, S. F., D. D. Durda, B. A. S. Gustafson, S. Jayaraman, J. C. Liou, and Y. L. Xu 1994. Zodiacal dust bands. In *Asteroids, Comets, Meteors, 1993* (A. Milani, M. di Martino, and A. Cellino, Eds.), pp. 127–142. Kluwer Dordrecht.
- Fillius, R. W., C. E. McIlwain, and A. Mogro-Campero 1975. Radiation belts of Jupiter: A second look. *Science* **188**, 465–467.
- Graham, J. R., K. Matthews, B. T. Soifer, J. Nelson, W. Harrison, G. Jernigan, S. Lin, G. Neugebauer, G. Smith, and C. Ziomkowski 1994. Infrared observations of the $z = 3.8$ radio galaxy 4C41.17 with the W. M. Keck Telescope. *Astrophys. J. Lett.* **420**, L5–L8.
- Hamilton, D. P. 1994. A comparison of Lorentz, planetary gravitational, and satellite gravitational resonances. *Icarus* **109**, 221–240.
- Horanyi, M., and T. E. Cravens 1996. The structure and dynamics of Jupiter's ring. *Nature* **381**, 293–295.
- Jewitt, D. C., and G. E. Danielson 1981. The jovian ring. *J. Geophys. Res.* **86**, 8691–8697.
- Jewitt, D. C., G. E. Danielson, and R. J. Terrile 1981. Groundbased observations of the jovian ring and inner satellites. *Icarus* **48**, 536–539.
- Matthews, K., and B. T. Soifer 1994. The near-infrared camera on the W. M. Keck Telescope. In *Infrared Arrays in Astronomy: The Next Generation* (I. S. McClean, Ed.), pp. 239–246. Kluwer, Dordrecht.
- Neugebauer, G., E. E. Becklin, D. Jewitt, R. Terrile, and G. E. Danielson 1981. Spectra of the jovian ring and Amalthea. *Astron. J.* **86**, 607–610.
- Nicholson, P. D., and K. Matthews 1991. Near-infrared observations of the jovian ring and small satellites. *Icarus* **93**, 331–346.
- Ockert-Bell, M. E., J. A. Burns, I. J. Dauber, P. C. Thomas, J. Veverka, M. J. S. Belton, and K. P. Klaasen 1999. The structure of Jupiter's ring system as revealed by the Galileo imaging experiment. *Icarus* **138**, 188–213.
- Owen, T., G. E. Danielson, A. F. Cook, C. Hansen, V. L. Hall, and T. C. Duxbury 1979. Jupiter's rings. *Nature* **281**, 442–446.
- Persson, S. E., D. C. Murphy, W. Krzeminski, M. Roth, and M. J. Rieke 1998. A new system of faint near-infrared standard stars. *Astron. J.* **116**, 2475–2488.
- Schaffer, L. E., and J. A. Burns 1992. Lorentz resonances and the vertical structure of dusty rings: Analytical and numerical results. *Icarus* **96**, 65–84.
- Showalter, M. R., J. A. Burns, J. N. Cuzzi, and J. B. Pollack 1985. Discovery of Jupiter's gossamer ring. *Nature* **316**, 526–528.
- Showalter, M. R., J. A. Burns, J. N. Cuzzi, and J. B. Pollack 1987. Jupiter's ring system: New results on structure and particle properties. *Icarus* **69**, 458–498.
- Showalter, M. R., J. N. Cuzzi, and S. M. Larson 1991. Structure and particle properties of Saturn's E Ring. *Icarus* **94**, 451–473.
- Smith, B. A., and H. J. Reitsemma 1980. CCD observations of Jupiter's ring and Amalthea. Presented at *IAU Colloquium 57, Kona, Hawaii*.
- Smoluchowski, R. 1976. Origin and structure of Jupiter and its satellites. In *Jupiter* (T. Gehrels, Ed.), pp. 3–21. Univ. of Arizona Press, Tucson.
- Thomas, P. C., J. A. Burns, L. Rossier, D. Simonelli, J. Veverka, C. R. Chapman, K. P. Klaasen, and M. J. S. Belton 1998. Small inner satellites of Jupiter. *Icarus* **135**, 360–371.